Wideband Cyclostationary Spectrum Analysis for Smart Factory Wireless Channels

Peter Vouras
U.S. Department of Defense
Washington, D.C., USA
Email: synthetic-aperture-twg@ieee.org

Mohamed Kashef (Hany) and Richard Candell
National Institute of Standards and Technology
Gaithersburg, MD., USA
Email: mohamed.kashef, rick.candell@nist.gov

***Abstract*—Smart and highly automated factories rely on time sensitive networks (TSNs) to coordinate the actions of robots working together to complete a task. The dense layout of metallic objects on the factory floor creates a complex electromagnetic environment with long-duration multipath. Furthermore, the motion of the robotic workers and the use of multi-carrier waveforms, such as Orthogonal Frequency Division Multiplexing (OFDM), limit the coherence time of the channel. In this paper, we propose a technique for characterizing the frequency behavior of wireless channels in industrial settings. Our proposed algorithm relies on detecting cyclostationary spectral features and includes a novel method for combining the frequency bins of a spectrogram. Cyclostationary feature detection is especially useful for integrating a sensing capability and the communication function of a wireless network. Synthetic aperture sounding measurements of the wireless channel within a utility plant are used to evaluate the proposed algorithm.**

I. Introduction

Emerging fifth and sixth generation (5G and 6G) wireless technologies are evolving to meet stringent data throughput and latency demands [1]. These technologies are also being leveraged to integrate a sensing capability. In the manufacturing market, automated factories rely on the reliability of time-sensitive networks (TSNs) to coordinate the actions of multiple robots working together in an assembly pipeline. A component of the ongoing research for bringing mechatronics to reality is deploying new techniques for measuring and characterizing the wireless environment in factory settings and detecting perturbations to the channel impulse or frequency response that indicate the presence of new objects. The industrial locations exhibit severe multipath and extraneous scattering due to the high density of metallic objects in the environment.

Emerging 6G networks will measure sensing primitives to determine the presence of unexpected objects or motion in the scene between the transmitter and receiver [2]. Examples of sensing primitives include a time series of received signal strength versus delay known as the channel impulse response (CIR), or an estimate of the received signal power versus frequency known as the channel frequency response (CFR). Both the CIR and the CFR can be estimated from training fields in the transmitted data packets. One category of sensing algorithms relies on comparing measured sensing primitives to an a priori model of the channel to detect any differences that can be attributed to new objects or motion. For this approach to be successful, an accurate baseline version of the channel is necessary. This paper describes a technique for extracting highly accurate cyclostationary features from synthetic aperture channel sounding measurements made in a static wireless channel in a factory setting. These features can then be compared against real-time measurements to detect unexpected perturbations.

Synthetic apertures have been explored in various channel sounding configurations for a number of years [3–13]. Synthetic aperture channel sounders utilize a mechanical positioner to move an antenna through space and collect phase coherent samples of the ambient wavefield that can be combined in post-processing to create high-resolution snapshots of the RF channel impulse response. The area of the synthetic aperture will determine the width of the mainbeam after Fourier beamforming and hence the angular resolution. The delay resolution will be inversely proportional to the measurement bandwidth and is especially important in scenarios where many closely spaced signal echoes must be differentiated. The use of vector network analyzers (VNAs) as wideband receivers for channel sounders has been described in several papers [14–20].

The measurement results described in this paper were collected using the SAMURAI synthetic aperture system developed by the National Institute of Standards and Technology (NIST) in Boulder, CO [21–24]. This system was used to collect wireless channel measurements inside the Central Utility Plant (CUP) located on the NIST campus in Boulder, CO. As illustrated in Fig. 1, the CUP is an exemplary location for analyzing the electromagnetic scattering conditions that would exist in a factory. Section II describes our algorithm and provides outputs using data measured by SAMURAI in the CUP.

II. Cyclostationary Feature Detection

In general, given the power spectral density (PSD) computed for a wide frequency range, it is difficult to determine the presence of a signal or to identify spectral features using energy detection. Furthermore, if a lump of energy is detected in the PSD, it is difficult to decide if this bump represents one or more signals. An alternative approach to energy detection is to look for cyclostationary features of signals.

Most signals have cyclostationary properties due to their modulation. Furthermore, time-varying channels with inherent motion and Doppler may also exhibit cyclostationary behavior. A useful property is that white or uncorrelated noise does not have any cyclostationary features. This property is relevant in industrial environments since diffuse multipath is highly random and uncorrelated from sample to sample, as is white noise.

Using the true time delay beamforming algorithm described in [24], we can band-partition the channel frequency response measured by SAMURAI for a particular spatial direction using a filter-bank and look for cyclostationary features at the center of each frequency bin. The magnitude squared of the inverse Fourier transform of the measured channel frequency response yields an estimate of the received power (normalized to transmit power) as a function of delay. This time series is also known as a power delay profile (PDP) and an example is shown in Fig. 2. The second advantage of cyclostationary signal analysis is that it decomposes the channel in both the time and frequency domains simultaneously.

Denote as $X[f_k]$ the complex CFR measured by SAMURAI on a discrete frequency grid of $K = 1351$ samples evenly spaced 10 MHz apart between 26.5 and 40 GHz. Let $x[n]$ represent the inverse Fourier transform of $X[f_k]$. The first step of the algorithm computes a windowed spectrogram by partitioning $x[n]$ into segments of length $L = 64$ that overlap by $P = L/4$ points. The number of frequency bins will also be equal to L. The number of segments is equal to

$$N_{seg} = \left\lceil \frac{K - L}{L - P} \right\rceil \tag{1}$$

where the last segment is zero padded if necessary. Denote the partitioned data as $x[p, n]$ where $n = 0, \ldots, N_{seg} - 1$ is the index of each data segment and $p = 0, \ldots, L - 1$ is the sample index of each segment. Let $X[f_p, n]$ denote the Fast Fourier Transform (FFT) of $w[p]x[p, n]$ over the index p where $w[p]$ is a window function.

One shortcoming of the spectrogram is that signals spanning multiple frequency bins do not exhibit cyclostationary behavior in any one frequency bin. For example, in the case where the measurement bandwidth $B = 13.5$ GHz and $L = 64$, then with no windowing, the bin spacing is approximately 211 MHz. A narrowband 50 MHz feature would have a high response in the bin closest to its center frequency. But, a 2000 MHz feature would look like noise in any individual frequency bin. Thus, it is necessary to combine frequency bins to look at cyclostationary behavior that spans several subbands.

The alternative to combining frequency bins, is to decrease the size of the DFT but this can have the unintended effect of decreasing frequency resolution too much. In this paper, we develop a novel technique for recombining frequency bins by sliding a window along the DFT output bins. Suppose it is desired to combine M frequency bins. Then the bandwidth of the bins will effectively increase by a factor of M so the temporal sampling rate of each frequency bin must be increased by M via interpolation. Let $\widehat{X}[f_p, \tilde{n}]$ denote the upsampled spectrogram where $0 \leq \tilde{n} \leq MN_{seg} - 1$. Next the center frequency of each bin is shifted to maintain the same relative spacing as in,

$$\tilde{X}[f_p, \tilde{n}] = \widehat{X}[f_p, \tilde{n}] e^{-\mathrm{j}\tilde{n}p/MN_{seg}}. \tag{2}$$

Finally, the outputs of M adjacent frequency bins are summed together as in,

$$\bar{X}[p_0, \tilde{n}] = \sum_{s=p_0}^{p_0+M-1} \tilde{X}[s, \tilde{n}] \tag{3}$$

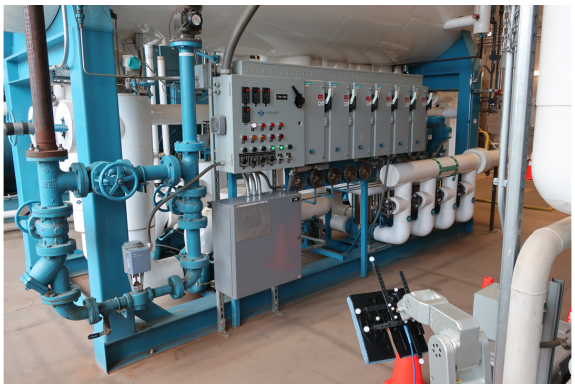

Figure 1. Picture showing synthetic aperture measurement in Central Utility Plant at NIST, Boulder, CO.

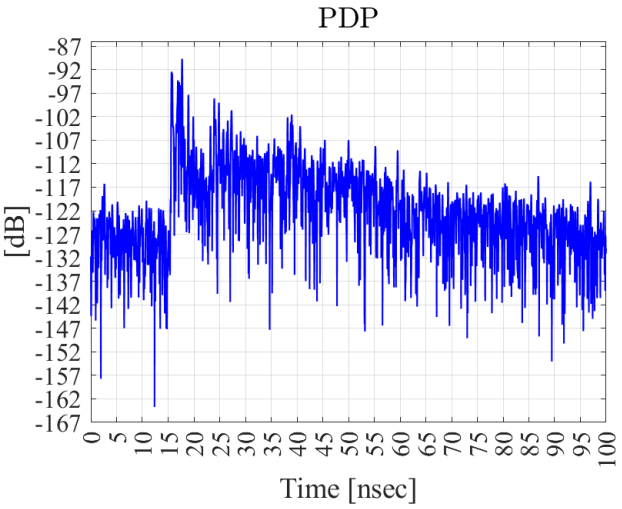

Figure 2. Power delay profile measured using a synthetic aperture. Plot shows long duration and strong diffuse component of multipath in industrial environments.

where $p_0 = 0, \ldots, L - M$. The result is the reconstructed baseband time series for a wider frequency range.

The cyclic detection statistic C_y is computed for each frequency bin of the final spectrogram. For a complex time series $y[n]$ of length N, C_y is defined as the mean of the absolute value of the auto-covariance sequence,

$$C_y = \frac{1}{N} \sum_{n=0}^{N-1} |\widehat{\kappa}_y[n]|, \tag{4}$$
$$\widehat{\kappa}_y[n] = \frac{1}{N} \sum_{i=0}^{N-1-|n|} (y[i] - \widehat{\mu}_y)(y[i + |n|] - \widehat{\mu}_y)^*.$$

Here $\widehat{\mu}_y$ denotes the sample mean and * represents complex conjugation.

Fig. 3 summarizes the cyclostationary feature detection algorithm. First we compute an overlapped, windowed, complex spectrogram of the PDP. The spectrogram is equivalent to a Discrete Fourier Transform (DFT) filter bank that yields the channelized and down-sampled version of $x[n]$ at L evenly-spaced center frequencies whose bandwidths are approximately B/L, where $B = 13.5$ GHz is the sample rate of the

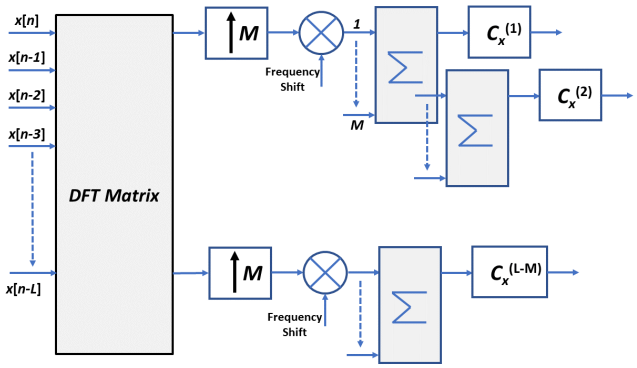

Figure 3. Processing chain showing polyphase implementation of a DFT filter bank, upsample operation in each sub-band, frequency shift, moving average across frequency bins, and computation of cyclic detection statistic.

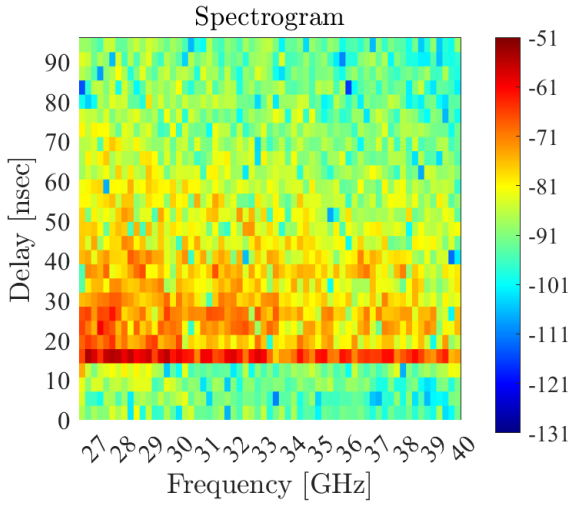

Figure 4. Spectrogram of complex PDP. The bandwidth of the channel measurement is 13.5 GHz between 26.5 and 40 GHz.

complex PDP $x[n]$ [24]. Fig. 4 illustrates the spectrogram of the PDP in Fig. 2 for the case where $M = 64$ and with 25% overlap between adjoining data segments.

A. Autoregressive Model of Multipath and Measured Results

As is clear in Fig. 2 that there is significant diffuse multipath energy in the measured PDP. The diffuse scattering can obfuscate spectral features and make it harder to characterize the channel. One approach to attenuate the received power of diffuse multipath is to apply a low-sidelobe taper to the spatial aperture. Another approach is to model the received multipath as an autoregressive (AR) random process.

Multipath consists of delayed replicas of the transmitted signal, thus it is well suited for AR modeling. An AR model of order Q represents the current sample of a signal $x[n]$ as a weighted combination of its Q previous samples plus an uncorrelated white-noise term $\nu[n]$ known as the innovation sequence,

$$x[n] = -a_1 x[n-1] - \ldots - a_Q x[n-Q] + \nu[n]. \quad (5)$$

The coefficients a_k are model parameters and can be obtained by solving the the Yule-Walker equations. An AR model is

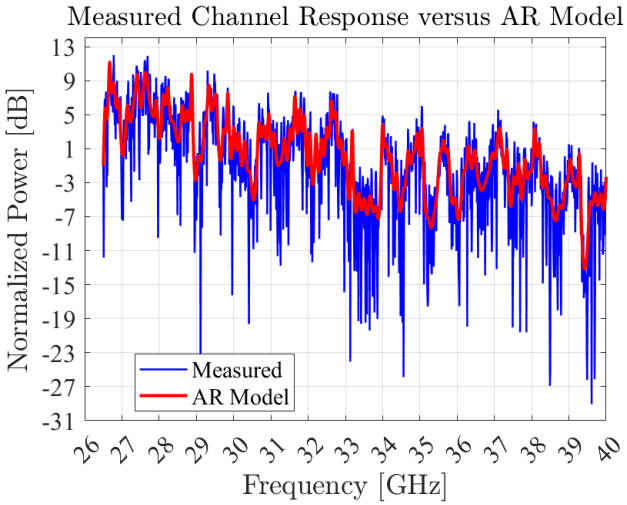

Figure 5. Plots showing close agreement between the AR model of multipath and measured data; P = 100.

also an all-pole filter that when excited with the white noise sequence $\nu[n]$ will produce an AR signal whose statistics match those of the given signal, $x[n]$. The complex frequency response of the all-pole filter evaluated at discrete angular frequency points $0 \leq \omega_l < 2\pi$ is given by

$$H(e^{\mathrm{j}\omega_l}) = \sum_{k=0}^{Q-1} \frac{1}{a_k e^{-\mathrm{j}k\omega_l}}. \quad (6)$$

The AR time series $x[n]$ is recovered by computing the inverse Fourier transform of $H(e^{\mathrm{j}\omega_l})$.

In order to solve the Yule-Walker equations, it is necessary to estimate the autocorrelation function of $x[n]$. The Levinson algorithm is then used to solve the Yule-Walker equations in an efficient manner [25] (pp. 524-529). Fig. 5 illustrates an AR model for the PDP in Fig. 2 for the case where $Q = 100$. Higher values of Q yield additional accuracy but the plot shows that the AR model has captured all the peaks and valleys in the data caused by the contributions from strong discrete scatterers that combine in and out of phase as the frequency increases. The AR model is used to generate the spectrogram shown in Fig. 6 and the accompanying frequency slice in Fig, 7 and the delay slice in Fig. 8.

The band partitioned filter bank outputs of the raw data were used to compute the cyclic detection statistic C_y in each composite frequency bin. Fig. 9 illustrates the cyclic detection statistic for the output of the AR model of the PDP. A very clear downward trend is evident in the plot along with a hump between 31 to 33 GHz. This plot is much smoother than the version constructed directly from the raw data due to the use of the AR model.

The red plot in Fig. 9 is normalized to account for the frequency dependent gain of the transmit and receive antennas. The Friis equation provides that the signal-to-noise-ratio (SNR) at the receive antenna of a bistatic channel sounder is given by

$$SNR = \frac{P_t G_t G_r \sigma \lambda^2}{(4\pi)^3 k T_s B R_t{}^2 R_r{}^2} \quad (7)$$

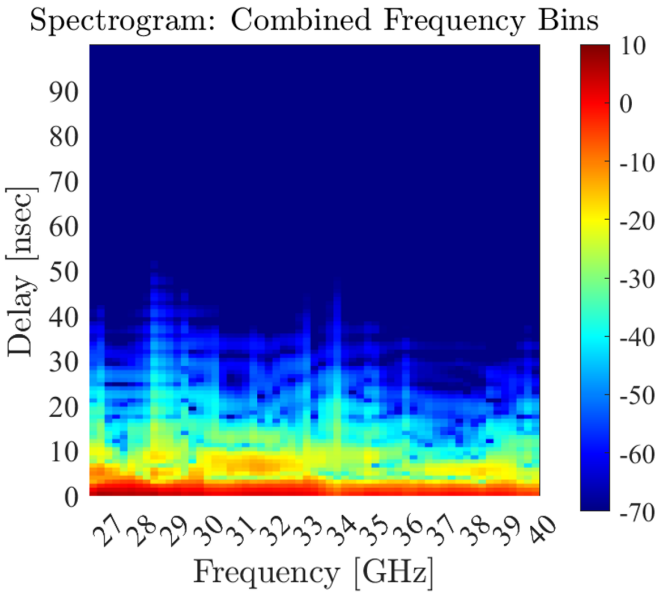

Figure 6. Spectrogram output for $L = 4$ combined frequency bins using the AR model output.

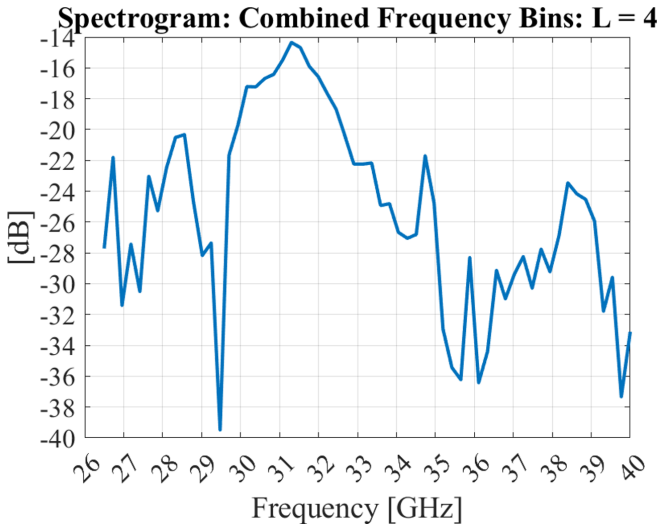

Figure 7. Frequency slice through spectrogram of AR model: $L = 4$ frequency bins combined with overlap.

where R_t is the distance from the transmit antenna to the scatterer, R_r is the distance from the scatterer to the receive antenna, P_t is the transmit power, G_t is the transmit antenna gain, G_r is the receive antenna gain, λ is the wavelength, σ is the bistatic cross sectional area of the scatterer, k is Boltzmann's constant, T_s is the receiver noise temperature, and B is the receiver noise bandwidth. Both the transmit and receive antennas have a fixed effective aperture area A_e that is related to the gain by

$$G = \frac{4\pi A_e}{\lambda^2}. \tag{8}$$

Substituting (8) into (7) for G_t and G_r shows that for fixed areas of the transmit and receive antennas, the received SNR will be inversely proportional to λ^2. Therefore to compensate for the frequency dependence of the product $G_t G_r$, the cyclic

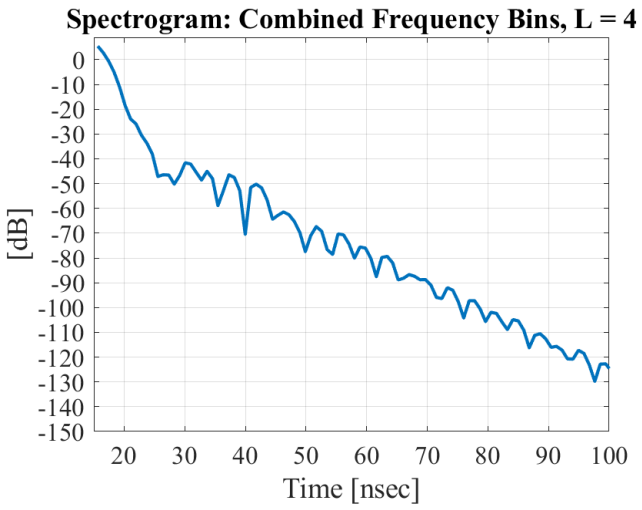

Figure 8. Delay slice through spectrogram of AR model: $L = 4$ frequency bins combined with overlap.

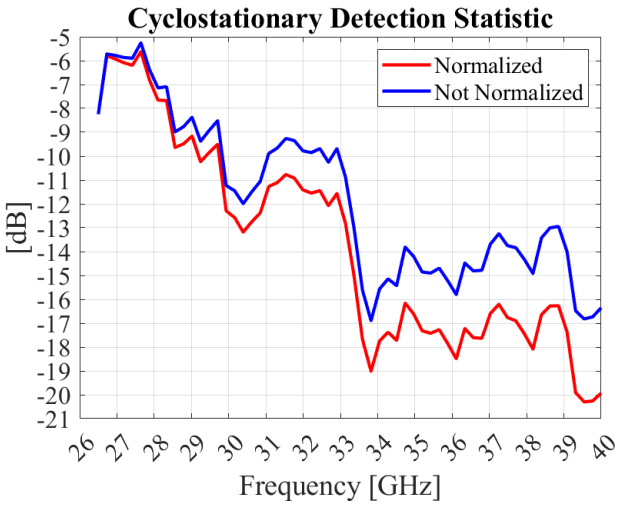

Figure 9. Final cyclostationary detection statistic computed from the AR model with and without antenna gain normalization.

detection statistic shown by the blue curve in Fig. 9 is multiplied by the factor λ^2/λ_0^2 where λ_0 corresponds to the wavelength at 26.5 GHz.

III. Conclusion

This paper demonstrates a technique to combine frequency bins in a spectrogram and to search for cyclostationary features in a wireless channel measured using a synthetic aperture. An AR model of the multipath mitigates the random variability caused by diffuse multipath and after normalizing for the frequency dependent gain of the transmit and receive antennas, the final results reveal clear trends in the data. The proposed algorithm can be used to support an integrated sensing and communication capability that detects new objects or motion in the environment by comparing a measured estimate of the CFR to an a priori model.

DISCLAIMER

Certain commercial equipment, instruments, or materials are identified in this paper in order to specify the experimental procedure adequately. Such identification is not intended to imply recommendation or endorsement by the National Institute of Standards and Technology, nor is it intended to imply that the materials or equipment identified are necessarily the best available for the purpose.

REFERENCES

[1] "Beyond 5G/6G KPIs and target values," in *whitepaper of the 5G Public Private Partnership: Test, Measurement and KPIs Validation Working Group*, 2022, pp. 1–53.

[2] C. C. F. Meneghello, C. Chenx and F. Restuccia, "Towards integrated sensing and communications in ieee 802.11bf wi-fi networks," *Arxiv*, vol. 2212.13930, pp. 1–6, 2022.

[3] S. Ranvier, M. Kyro, K. Haneda, T. Mustonen, C. Icheln, and P. Vainikainen, "VNA-Based wideband 60 GHz MIMO channel sounder with 3-D arrays," in *IEEE Radio and Wireless Symposium*, 2009.

[4] H. Nguyen, K. Mahler, M. Peter, W. Keusgen, T. Eichler, and H. Mellein, "Estimation of DoA based on large scale virtual array data," in *10th European Conference on Antennas and Propagation*, 2016.

[5] H. Nguyen, W. Keusgen, and T. Eichler, "Instantaneous direction of arrival measurements in mobile radio channels using virtual circular array antennas," in *IEEE Global Communications (Globecom) Workshops*, 2016.

[6] H. Hayashi and T. Ohtsuki, "DOA estimation in MIMO radar using temporal spatial virtual array with music algorithm," in *9th International Conference on Signal Processing and Communication Systems*, 2015.

[7] A. Mannesson, B. Bernhardsson, M. Yaqoob, and T. F, "Optimal virtual array length under position imperfections," in *IEEE 8th Sensor Array and Multichannel Signal Processing Workshop*, 2014.

[8] M. H. C. Dias and G. L. Siqueira, "Indoor 1.8 GHz AOA-TDOA measurements extending the use of a wideband propagation channel sounder with the synthetic aperture concept," in *European Microwave Conference*, 2005.

[9] H. Qiao, P. Sarangi, Y. Alnumay, and P. Pal, "Sample complexity tradeoffs for synthetic aperture based high resolution estimation and detection," in *IEEE 11th Sensor Array and Multichannel Signal Processing Workshop*, 2020.

[10] A. W. Mbugua, W. Fan, Y. Ji, and G. F. Pedersen, "Millimeter wave multi-user performance evaluation based on measured channels with virtual antenna array channel sounder," *IEEE Access*, vol. 6, 2018.

[11] B. Chen, Z. Zhong, B. Ai, and D. G. Michelson, "Moving virtual array measurement scheme in high-speed railway," *IEEE Antennas and Wireless Propagation Letters*, vol. 15, 2015.

[12] T. Zhou, C. Tao, S. Salous, and L. Liu, "Measurements and analysis of angular characteristics and spatial correlation for high-speed railway channels," *IEEE Transactions on Intelligent Transportation Systems*, vol. 19, no. 2, 2018.

[13] M. G. Becker, R. D. Horansky, D. Senic, V. Neylon, and K. A. Remley, "Spatial channels for wireless over-the-air measurements in reverberation chambers," in *12th European Conference on Antennas and Propagation*, 2018.

[14] J. A. Jargon, J. T. Quimby, K. A. Remley, A. A. Koepke, and D. F. Williams, "Verifying the performance of a correlation-based channel sounder in the 3.5 GHz band with a calibrated vector network analyzer," in *IEEE Asia-Pacific Microwave Conference (APMC)*, 2019.

[15] G. Santella and E. Restuccia, "Analysis of frequency domain wide-band measurements of the indoor radio channel at 1, 5.5, 10 and 18 GHz," in *IEEE Global Communications (Globecom) Conference*, 1996.

[16] S. J. Howard and K. Pahlavan, "Measurement and analysis of the indoor radio channel in the frequency domain," *IEEE Transactions on Instrumentation and Measurement*, vol. 39, no. 5, 1990.

[17] M. Kyro, S. Ranvier, V. M. Kolmonen, K. Haneda, and P. Vainikainen, "Long range wideband channel measurements at 81-86 GHz frequency range," in *4th European Conference on Antennas and Propagation*, 2020.

[18] J. Hejselbaek, W. Fan, and G. F. Pedersen, "Ultrawideband VNA based channel sounding system for centimetre and millimetre wave bands," in *27th IEEE Annual International Symposium on Personal, Indoor, and Mobile Radio Communications (PIMRC)*, 2016.

[19] A. M. Street, L. Lukama, and D. J. Edwards, "Use of VNAs for wideband propagation measurements," *IEE Proceedings on Communications*, vol. 148, no. 6, 2001.

[20] C. U. Bas, V. Kristem, R. Wang, and A. F. Molisch, "Real-time ultra-wideband channel sounder design for 3-18 GHz," *IEEE Transactions on Communications*, vol. 67, no. 4, 2019.

[21] A. J. Weiss, D. F. Williams, J. Quimby, R. Leonhardt, T. Choi, Z. Cheng, K. A. Remley, A. Molisch, B. Jamroz, J. Rezac, P. Vouras, and C. Zhang, "Large-signal network analysis for over-the-air test of up-converting and down-converting phased arrays," in *2019 IEEE MTT-S International Microwave Symposium (IMS) Digest*, 2019.

[22] A. J. Weiss, J. Quimby, R. Leonhardt, B. Jamroz, D. Williams, K. Remley, P. Vouras, and A. Elsherbeni, "Setup and control of a millimeter-wave synthetic aperture measurement system with uncertainties," in *95th Automatic Radio Frequency Techniques Group (ARFTG) Microwave Measurement Conference*, 2020.

[23] P. Vouras, K. A. Remley, B. Jamroz, M. Becker, D. F. Williams, J. Quimby, R. Leonhardt, R. D. Horansky, A. Weiss, R. D. Jones, J. Kast, A. Elsherbeni, P. Manurkar, D. Guven, J. Chuang, and C. Gentile, *Metrology for 5G and Emerging Wireless Technologies; T. Loh ed.* IET, 2021.

[24] P. Vouras, B. Jamroz, A. Weiss, D. F. Williams, R. Leonhardt, D. Guven, R. Jones, J. Kast, K. A. Remley, R. D. Horansky, and C. Gentille, "Wideband synthetic-aperture millimeter-wave spatial-channel reference system with traceable uncertainty framework," *IEEE Open Journal of Vehicular Technology*, vol. 4, pp. 325–341, 2023.

[25] B. Porat, *A Course in Digital Signal Processing*. John Wiley and Sons, 1997.